ISSN 2618-1584 Vol. 8, Issue 2: 49-58, DOI: 10.25236/FMSR.2026.080207

A Novel Immune-Related Four-Gene Signature for Prognosis and Immune Infiltration in Lung Adenocarcinoma

Nan Wu[1,a], Linyong Du[2,b,*]

[1]College of Laboratory Medicine and Life Science, Wenzhou Medical University, Wenzhou, Zhejiang, China
[2]Key Laboratory of Laboratory Medicine, Ministry of Education, College of Laboratory Medicine and Life Science, Wenzhou Medical University, Wenzhou, Zhejiang, 325035, China
[a]nanwu2026@163.com, [b]dullyong@163.com
**Corresponding author*

Abstract: *Lung adenocarcinoma (LUAD) remains a leading cause of cancer-related mortality worldwide, highlighting an urgent need for robust prognostic biomarkers to guide clinical decision-making. In this study, we integrated single-cell RNA sequencing (GSE131907) with bulk transcriptomic data from The Cancer Genome Atlas (TCGA)-LUAD cohort to construct an immune-related prognostic signature. Through comprehensive analysis of 86,145 single cells, we established a LUAD atlas and identified immune-related genes by intersecting single-cell markers with the ImmPort database. Univariate Cox regression and LASSO penalized Cox analysis revealed a four-gene signature comprising PITX3, DKK1, TLE1, and LDHA, which stratified patients into high- and low-risk groups with significantly different overall survival outcomes (Log-rank P < 0.001). The signature exhibited robust predictive accuracy with area under the curve values of 0.713, 0.695, and 0.640 for 1-, 3-, and 5-year survival, respectively. Immune infiltration analysis using the xCell algorithm demonstrated that the low-risk group was enriched with anti-tumor immune cells, including CD8+ T cells and dendritic cells, while the high-risk group showed higher infiltration of immunosuppressive components. Furthermore, the risk score was positively correlated with immune checkpoint molecules such as PDCD1 and LAG3, suggesting an association with T-cell exhaustion and immune evasion. In summary, this four-gene immune-related signature serves as a promising prognostic biomarker for LUAD, offering valuable insights into the tumor immune microenvironment and potential implications for personalized immunotherapy strategies.*

Keywords: *Lung Adenocarcinoma; Prognostic Signature; Single-Cell Analysis; Immune Checkpoint*

1. Introduction

Lung cancer remains one of the most prevalent and deadliest malignancies worldwide, with non-small cell lung cancer (NSCLC) accounting for approximately 85% of all lung cancer cases, and lung adenocarcinoma (LUAD) being its most common histological subtype [1]. Clinically, about one-third of NSCLC patients are diagnosed at an early stage (stage I–IIIA) eligible for surgical resection [2]. However, postoperative micro-metastatic foci are often resistant to conventional chemotherapy or radiotherapy, ultimately leading to tumor recurrence or distant metastasis [3]. In recent years, the emergence of immunotherapy has revolutionized the therapeutic landscape of NSCLC. Immune checkpoint inhibitors (ICIs) restore the effector function of exhausted T cells and have demonstrated significant clinical benefits in both advanced and resectable NSCLC [3]. Whether as monotherapy targeting programmed cell death protein 1 and its ligand (PD-1/PD-L1), dual blockade combining PD-1 with cytotoxic T-lymphocyte-associated protein 4 (CTLA-4), or in combination with chemotherapy, these strategies as neoadjuvant or adjuvant immunotherapies have effectively improved pathological response rates and prolonged patient survival [4-6]. Nevertheless, a considerable proportion of patients exhibit primary or acquired resistance to immunotherapy, the underlying mechanisms of which remain incompletely understood. Hence, there is an urgent need to develop novel biomarkers capable of accurately predicting prognosis and immunotherapeutic response in NSCLC.

The composition and functional status of the tumor immune microenvironment (TIME) are closely

ISSN 2618-1584 Vol. 8, Issue 2: 49-58, DOI: 10.25236/FMSR.2026.080207

linked to tumor progression and immunotherapy response [7]. Advances in single-cell RNA sequencing (scRNA-seq) have enabled the dissection of TIME heterogeneity at single-cell resolution, revealing the roles of distinct immune cell subsets in tumorigenesis [8]. As core regulators of immune responses, immune-related genes exhibit expression patterns that are intimately associated with TIME features and may serve as potential prognostic markers or therapeutic targets [9,10]. This study aims to integrate scRNA-seq data with bulk transcriptomic data from public databases to systematically identify key genes associated with the NSCLC immune microenvironment, construct and validate a robust immune-related prognostic signature, and explore its associations with immune cell infiltration and immune checkpoint molecules, thereby providing new theoretical insights and molecular targets for risk stratification and personalized immunotherapy in NSCLC.

Through integrated analysis of single-cell and bulk transcriptomic data, we systematically characterized the expression profiles of immune-related genes in the NSCLC microenvironment. Using univariate Cox regression and LASSO regression analyses, we ultimately identified four immune-related genes (PITX3, DKK1, TLE1, and LDHA) that were closely associated with patient prognosis and constructed a novel prognostic signature based on them. This signature exhibited favorable predictive performance across multiple datasets and was significantly correlated with tumor immune microenvironment characteristics, suggesting its potential as a reference for risk stratification and individualized immunotherapy in NSCLC.

2. Materials and Methods

2.1. Data Acquisition and Preprocessing

The single-cell RNA sequencing dataset GSE131907 was downloaded from the Gene Expression Omnibus (GEO) database, which contains samples from patients with non-small cell lung cancer (NSCLC) [11]. The raw count matrix was extracted and processed using the Seurat package (v4.3.0) in R. Quality control was performed to exclude low-quality cells with mitochondrial gene percentage >5%, detected genes <200 or >2500. After normalization and scaling, principal component analysis (PCA) was conducted, and the first 20 principal components were used for clustering and uniform manifold approximation and projection (UMAP) visualization. Cell types were annotated based on canonical marker genes and previously curated annotations provided with the dataset, ultimately constructing a comprehensive single-cell atlas encompassing epithelial cells, T cells, B cells, macrophages, fibroblasts, endothelial cells, and other immune subsets.

2.2. Identification of Immune-Related Genes

A list of immune-related genes was obtained from the ImmPort database (https://www.immport.org/shared/genelists). Additionally, the C7 immunologic signature gene set collection from the Molecular Signatures Database (MSigDB) was retrieved using the msigdbr R package. Only genes with valid gene symbols were retained for subsequent analyses [12]. The intersection of genes expressed in the single-cell dataset and the immune gene sets was defined as immune-related candidate genes.

2.3. TCGA-LUAD Data Processing

RNA sequencing data and corresponding clinical information for lung adenocarcinoma (LUAD) were obtained from The Cancer Genome Atlas (TCGA) using the TCGAbiolinks R package [13]. Gene expression values were normalized and transformed to transcripts per million (TPM). Samples with incomplete survival data were excluded. Differential expression analysis between tumor and normal tissues was performed using the limma package on log2(TPM+1) transformed data. Genes with |log2 fold change| > 1 and adjusted P-value < 0.05 were considered significantly differentially expressed.

2.4. Construction of the Prognostic Signature

Univariate Cox regression analysis was performed using the survival package to evaluate the association between each immune-related gene and overall survival (OS). Genes with P-value < 0.05 were considered significant and subsequently subjected to least absolute shrinkage and selection operator (LASSO) Cox regression analysis using the glmnet package with family = "cox" and alpha = 1. Ten-fold cross-validation was employed to determine the optimal penalty parameter λ. Genes with non-zero

ISSN 2618-1584 Vol. 8, Issue 2: 49-58, DOI: 10.25236/FMSR.2026.080207

coefficients at the optimal λ were retained for further multivariable Cox regression analysis. The risk score for each patient was calculated as a linear combination of gene expression levels weighted by their corresponding coefficients. Patients were stratified into high-risk and low-risk groups based on the median risk score.

2.5. Evaluation of the Prognostic Model

Kaplan-Meier survival analysis with the log-rank test was performed using the survminer package to compare OS between the high-risk and low-risk groups. Time-dependent receiver operating characteristic (ROC) curves were generated using the timeROC package to assess the predictive accuracy of the risk score at 1, 3, and 5 years. The area under the curve (AUC) was calculated, with AUC > 0.65 considered acceptable predictive performance.

2.6. Immune Infiltration Analysis

The relative abundances of 64 immune and stromal cell types in each TCGA-LUAD sample were inferred using the xCell algorithm implemented in the xCell R package, with parameters set to rnaseq = TRUE for RNA-seq data [14]. The enrichment scores for each cell type were compared between the high-risk and low-risk groups using the Wilcoxon rank-sum test, and boxplots were generated to visualize cell types with significant differences ($P < 0.05$). Additionally, Pearson correlation analysis was performed to evaluate the associations between the risk score and key immune checkpoint molecules (PDCD1, CD274, CTLA4, LAG3), with results visualized using scatter plots and boxplots.

2.7. Single-Cell Validation of Prognostic Genes

To validate the expression patterns of the final prognostic genes at single-cell resolution, the GSE131907 dataset was reanalyzed. The expression distribution of each gene was visualized on UMAP plots using the FeaturePlot function in Seurat [14]. Dot plots were generated to illustrate the average expression levels and the proportion of expressing cells across major cell lineages, confirming the cell-type specificity of these genes.

2.8. Statistical Analysis

All statistical analyses were performed using R software (version 4.2.1). Continuous variables were compared using the Wilcoxon rank-sum test or Student's t-test, as appropriate. Survival differences were assessed using the log-rank test. Correlation analyses were conducted using Pearson or Spearman methods. A two-tailed P-value < 0.05 was considered statistically significant unless otherwise specified.

3. Results

3.1. Construction of the LUAD Single-Cell Atlas and Cell Type Annotation

To comprehensively characterize the cellular composition of non-small cell lung cancer, we performed single-cell transcriptomic analysis on 86,145 high-quality cells from the GSE131907 dataset. Through dimensionality reduction, clustering, and UMAP visualization, we identified major cell lineages, comprising 9 distinct cell types including epithelial cells, T cells, B cells, macrophages, fibroblasts, and endothelial cells (Fig. 1A). Validation using canonical marker genes confirmed the accuracy and reliability of cell subtype annotations (Fig. 1B). This atlas provides a foundation for subsequent immune-related gene screening and prognostic gene validation.

ISSN 2618-1584 Vol. 8, Issue 2: 49-58, DOI: 10.25236/FMSR.2026.080207

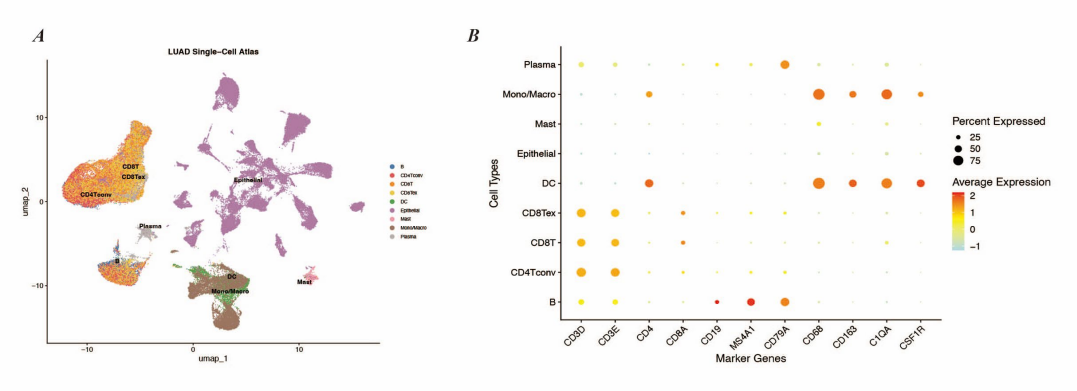

A: UMAP plot showing the distribution of major cell types in LUAD tissues, with each color representing a distinct cell lineage. B: Dot plot displaying the average expression levels (color intensity) and the proportion of expressing cells (dot size) of canonical marker genes across different cell types.

Figure 1. Construction of the LUAD Single-Cell Atlas and Cell Type Annotation.

3.2. Identification of Immune-Related Genes

To systematically identify immune-related genes with potential prognostic value in LUAD, we first intersected genes detected in the single-cell dataset with immune gene sets from the ImmPort database (or the MSigDB C7 collection). This analysis yielded a total of 4,065 immune-related genes expressed within the LUAD microenvironment (Fig. 2A). We then examined the differential expression of these genes between tumor and normal tissues using the TCGA-LUAD cohort. The volcano plot illustrates the overall expression landscape, highlighting genes that are significantly upregulated (red) or downregulated (blue) in LUAD (Fig. 2B). The identified immune-related genes encompass diverse functional categories—including cytokines, chemokines, co-stimulatory molecules, and immune checkpoints—providing a comprehensive candidate pool for subsequent survival-based screening.

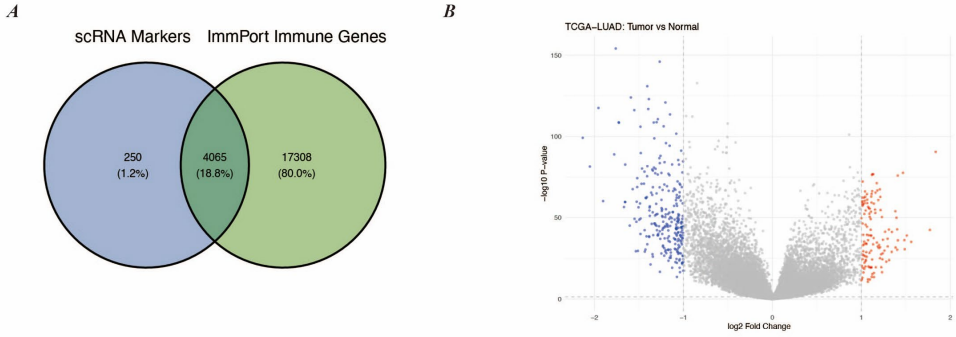

A: Venn diagram illustrating the overlap between genes expressed in single-cell data and immune gene sets. The number in the overlapping region represents the count of immune-related candidate genes. B: Volcano plot of differentially expressed genes between LUAD and normal tissues. Red dots indicate significantly upregulated genes, blue dots indicate significantly downregulated genes, and gray dots represent non-significant genes ($|log2FC| \leq 1$ or adjusted $P \geq 0.05$).

Figure 2. Identification of immune-related genes.

3.3. Univariate Cox Regression Analysis of Immune-Related Genes in the TCGA-LUAD Cohort

Based on 576 samples with complete survival information from the TCGA-LUAD cohort, we performed univariate Cox regression analysis on the aforementioned 4,065 immune-related genes. The results revealed that the expression levels of 3,883 genes were significantly associated with overall survival ($P < 0.05$) (Fig. 3A). Notably, all of the top 30 most significant genes exhibited hazard ratios (HR) greater than 1, indicating that high expression of these genes is closely associated with poor prognosis, such as PITX3, DKK1, LDHA, and TLE1. These findings suggest that the identified immune-

ISSN 2618-1584 Vol. 8, Issue 2: 49-58, DOI: 10.25236/FMSR.2026.080207

related genes primarily function as risk factors involved in NSCLC progression, potentially influencing patient survival through mechanisms including tumor proliferation, immune evasion, or metastasis.

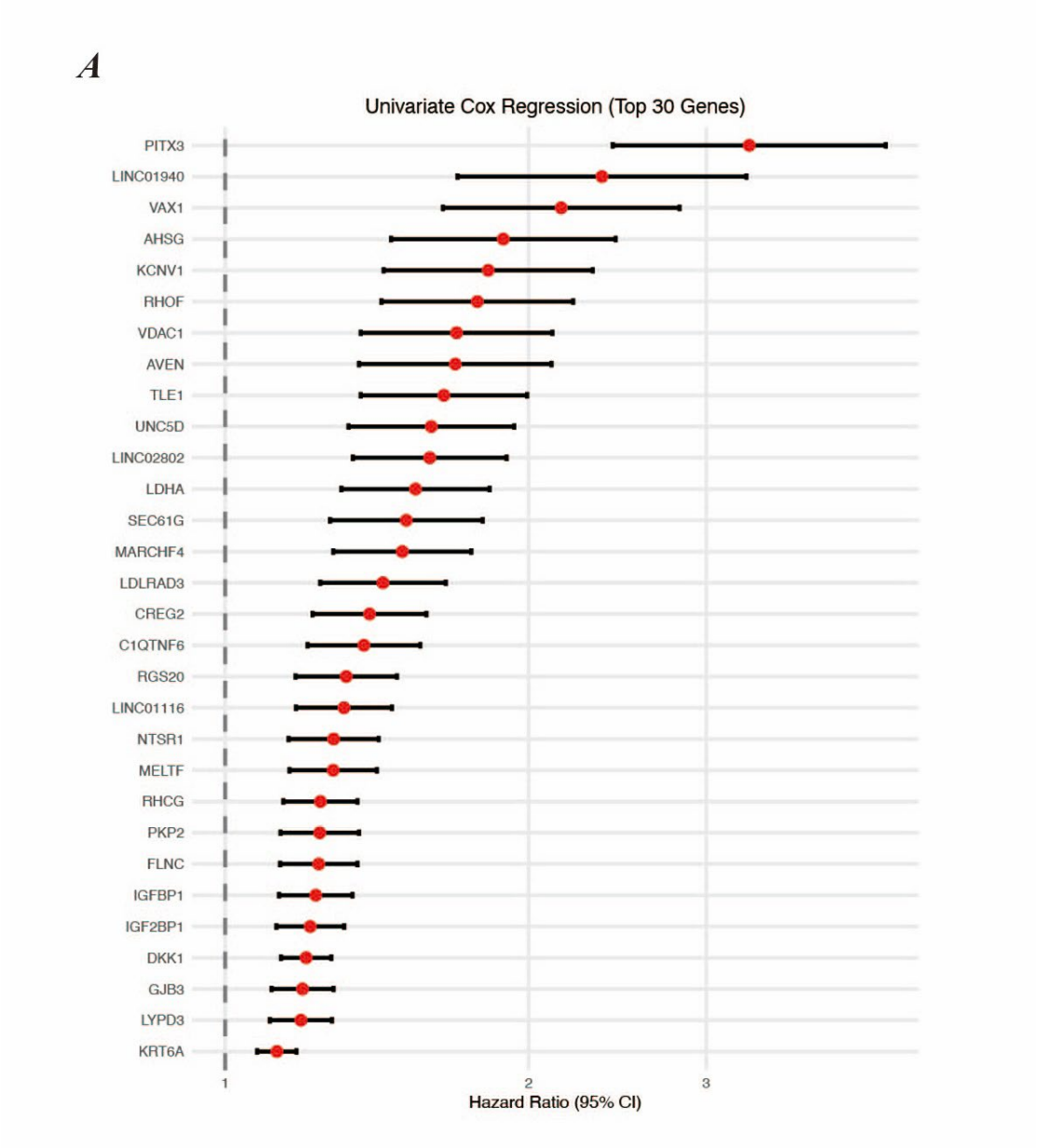

A: Forest plot showing the univariate Cox regression results for the top 30 most significant immune-related genes. Hazard ratios (HR) are represented by squares, with horizontal lines indicating 95% confidence intervals. Red indicates HR > 1 (risk factors), while blue indicates HR < 1 (protective factors).

Figure 3. Univariate Cox Regression Analysis of Immune-Related Genes in the TCGA-LUAD Cohort.

3.4. Construction of the Prognostic Signature Using LASSO Regression

To avoid overfitting and select the most representative prognostic genes, LASSO Cox regression analysis was performed on the 3,883 significant genes identified above. The optimal penalty parameter λ was determined through 10-fold cross-validation (Fig. 4A), ultimately identifying four genes with non-zero coefficients: PITX3, DKK1, TLE1, and LDHA (Fig. 4B-C). Multivariable Cox regression analysis revealed that all four genes were independent risk factors (P = 4.45e-05, 0.000201, 0.005056, and 0.015538, respectively). The risk score was calculated using the formula: Risk score = (0.738 × expression of PITX3) + (0.118 × expression of DKK1) + (0.282 × expression of TLE1) + (0.218 × expression of LDHA). Based on the median risk score, patients were stratified into high-risk and low-

ISSN 2618-1584 Vol. 8, Issue 2: 49-58, DOI: 10.25236/FMSR.2026.080207

risk groups.

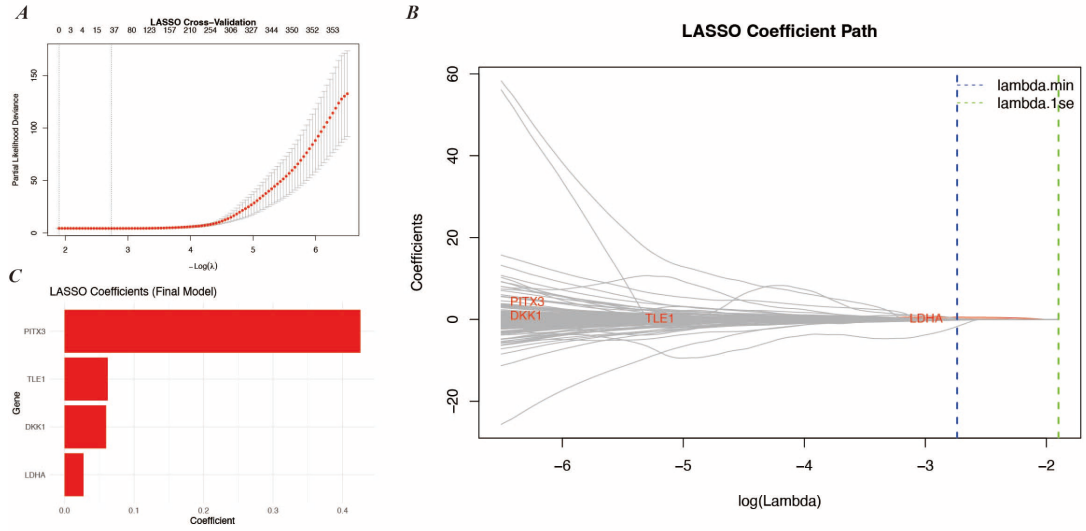

A: LASSO regression cross-validation curve showing the partial likelihood deviance under different λ values. The left dashed line indicates λ.min, and the right dashed line indicates λ.1se. B: LASSO coefficient path plot, where each curve represents the trajectory of a gene's coefficient as λ varies, with the vertical line corresponding to the optimal λ. C: Bar plot showing the coefficients of the four genes in the final model.

Figure 4. Construction of the Prognostic Signature Using LASSO Regression.

3.5. Survival Analysis and Performance Evaluation of the Prognostic Signature

Kaplan-Meier survival analysis demonstrated that patients in the high-risk group had significantly shorter overall survival compared to those in the low-risk group (log-rank test $P < 0.0001$, Fig. 5A). Time-dependent receiver operating characteristic (ROC) curve analysis indicated that the risk score exhibited favorable predictive ability for patient survival at 1, 3, and 5 years, with area under the curve (AUC) values of 0.713, 0.695, and 0.640, respectively (Fig. 5B). These results confirm that the 4-gene prognostic signature possesses robust risk stratification capacity and predictive accuracy in LUAD.

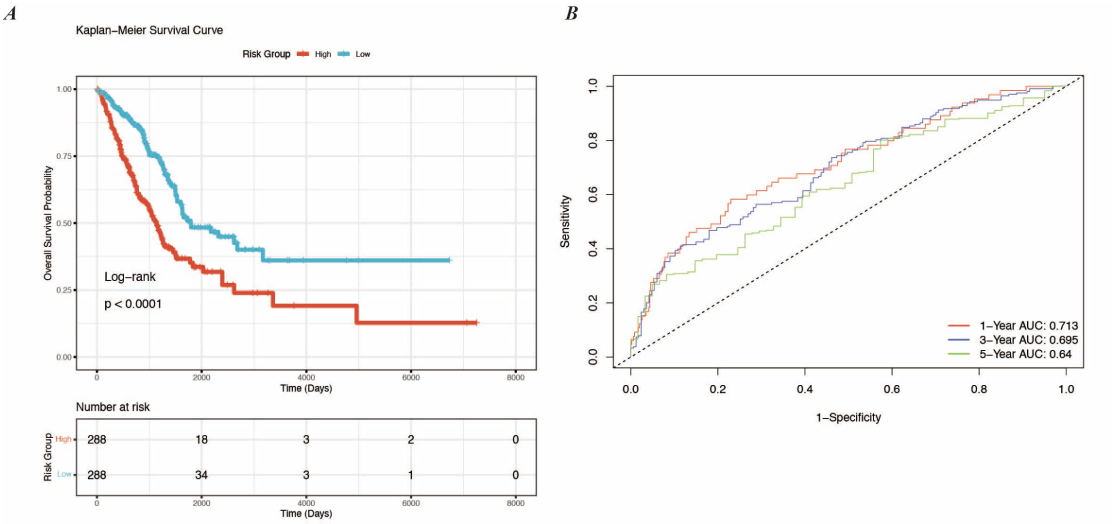

A: Kaplan-Meier survival curves for patients in the high-risk and low-risk groups. B: Time-dependent ROC curves of the risk score for predicting 1-, 3-, and 5-year survival.

Figure 5. Survival Analysis and Performance Evaluation of the Prognostic Signature.

3.6. Differential Immune Infiltration Analysis Between High-Risk and Low-Risk Groups

To investigate the relationship between the prognostic signature and the tumor immune

ISSN 2618-1584 Vol. 8, Issue 2: 49-58, DOI: 10.25236/FMSR.2026.080207

microenvironment, we evaluated the infiltration abundances of 64 immune and stromal cell types in TCGA-LUAD samples using the xCell algorithm and compared the differences between high-risk and low-risk groups. The results revealed that the low-risk group exhibited significantly higher infiltration levels of various adaptive immune cells, including CD8+ T cells, CD4+ T cells, dendritic cells (DCs), and neutrophils, compared to the high-risk group ($P < 0.05$, Fig. 6A-B). Conversely, the high-risk group showed enrichment of M1 macrophages, Th1/2 cells, and mesenchymal stem cells (MSCs). Furthermore, both the ImmuneScore and StromaScore were higher in the low-risk group than in the high-risk group, suggesting a "hotter" microenvironment with more complete stromal support. These findings indicate that the low-risk group may be in an immune-activated state conducive to antitumor immune responses.

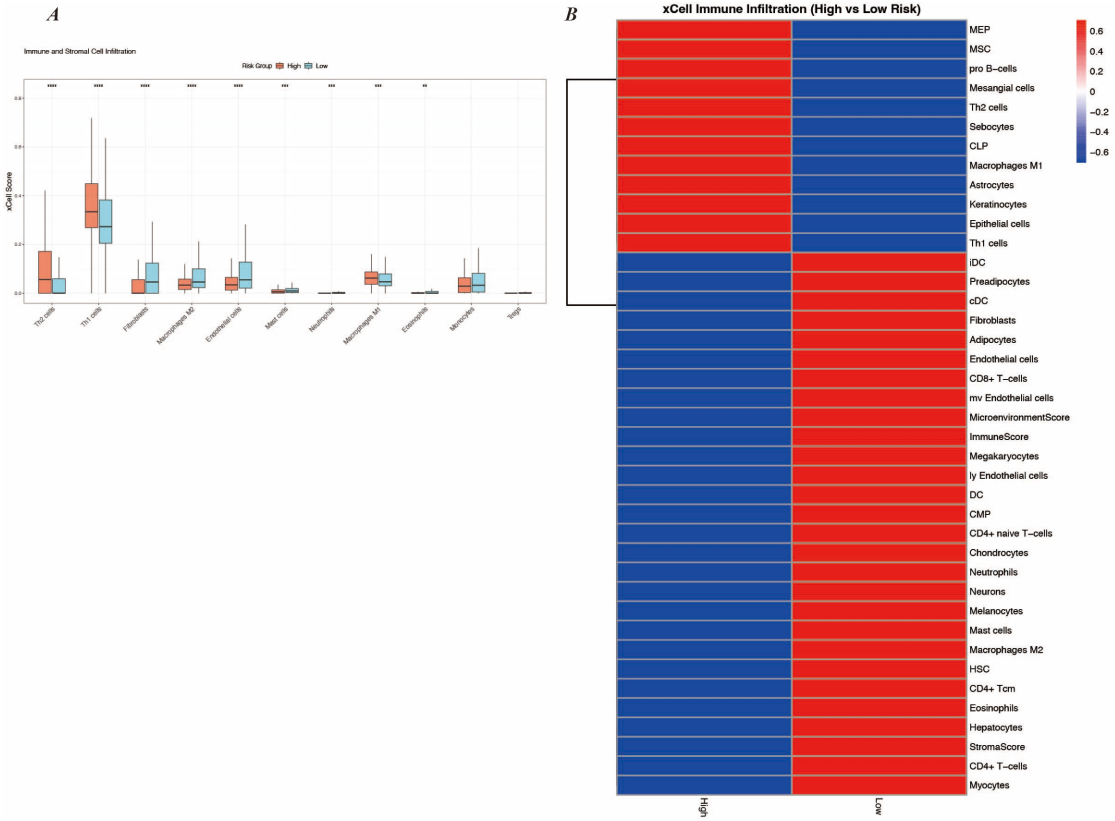

*A: Box plots showing the xCell scores of key immune and stromal cells with significant differences between high-risk and low-risk groups. Red represents the high-risk group, and blue represents the low-risk group. * $P < 0.05$, ** $P < 0.01$, *** $P < 0.001$. B: Heatmap displaying the mean infiltration scores of all 64 cell types, as well as ImmuneScore, StromaScore, and MicroenvironmentScore, in the high-risk and low-risk groups. Rows are scaled for visualization.*

Figure 6. Differential Immune Infiltration Analysis Between High-Risk and Low-Risk Groups.

3.7. Expression Analysis of Immune Checkpoint Molecules

Given that the low-risk group was enriched with more effector immune cells, we further analyzed the differential expression of immune checkpoint molecules between the high-risk and low-risk groups. The results demonstrated that immunosuppressive checkpoint molecules, including PDCD1 (PD-1) and LAG3, were significantly upregulated in the high-risk group compared to the low-risk group ($P < 0.05$, Fig. 7A). Correlation analysis revealed that the risk score exhibited weak but significant positive correlations with the expression of PDCD1 ($R = 0.11$, $P = 0.011$), LAG3 ($R = 0.096$, $P = 0.019$), and CD274 ($R = 0.14$, $P = 0.00062$), while no statistically significant correlation was observed with CTLA4 ($R = 0.022$, $P = 0.6$) (Fig. 7B). These findings suggest that the high-risk group may harbor more severe T-cell exhaustion and an immunosuppressive microenvironment.

ISSN 2618-1584 Vol. 8, Issue 2: 49-58, DOI: 10.25236/FMSR.2026.080207

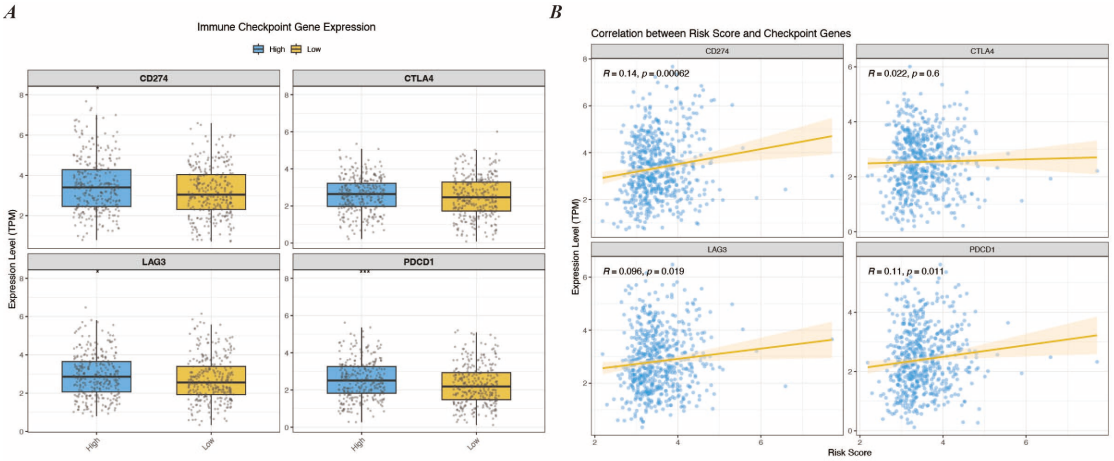

A: Box plots showing the expression levels of immune checkpoint molecules in high-risk and low-risk groups. B: Scatter plots illustrating the correlations between risk score and the expression of PDCD1, CTLA4, and LAG3, with blue lines representing linear regression fits and gray areas indicating 95% confidence intervals.

Figure 7. Association analysis between immune checkpoint molecule expression and risk score.

3.8. Single-Cell Validation of Prognostic Genes

Finally, we validated the expression patterns of the four prognostic genes (PITX3, DKK1, TLE1, and LDHA) in the GSE131907 single-cell atlas. UMAP feature plots revealed that LDHA was broadly expressed across multiple cell types, particularly enriched in tumor epithelial cells and certain myeloid cell populations. In contrast, PITX3, DKK1, and TLE1 exhibited relatively restricted expression patterns. Specifically, PITX3 was predominantly expressed in epithelial cell subsets, DKK1 was enriched in fibroblasts, while TLE1 was expressed in both T cells and subsets of epithelial cells (Fig. 8A-D). Dot plots further quantified the average expression levels and the proportion of expressing cells across major cell lineages, confirming the cell-type specificity of these genes (Fig. 8E). These findings provide insights into the potential cellular origins of the prognostic genes at single-cell resolution.

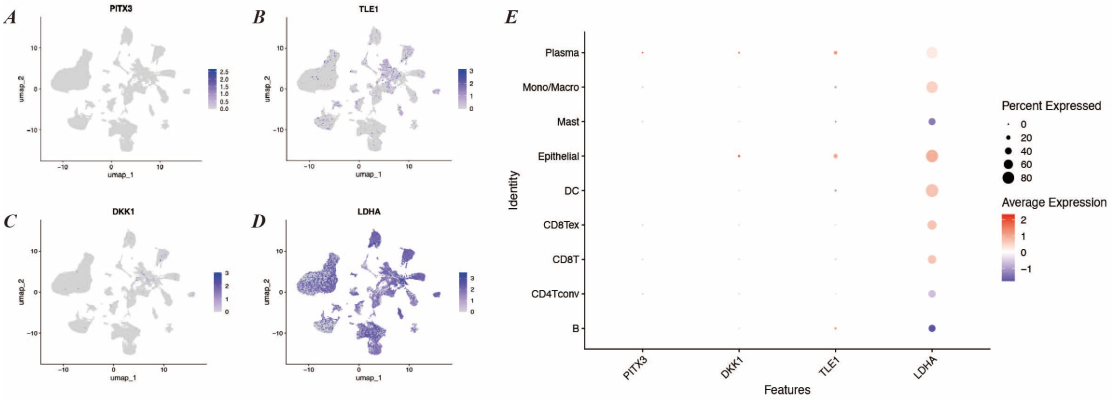

A-D: UMAP feature plots showing the expression distribution of PITX3 (A), DKK1 (B), TLE1 (C), and LDHA (D) in the single-cell atlas, respectively. Darker colors indicate higher expression levels. E: Dot plot displaying the average expression levels (color intensity) and the proportion of expressing cells (dot size) of the four genes across major cell lineages.

Figure 8. Single-Cell Validation of Prognostic Genes

4. Discussion

Lung adenocarcinoma (LUAD) remains a leading cause of cancer-related mortality worldwide, with high recurrence rates even after multimodal therapy. Although immune checkpoint inhibitors have revolutionized treatment, durable responses are limited to a subset of patients, underscoring the urgent need for reliable prognostic biomarkers to guide personalized strategies. In this study, we integrated

ISSN 2618-1584 Vol. 8, Issue 2: 49-58, DOI: 10.25236/FMSR.2026.080207

single-cell and bulk transcriptomic data to develop a four-gene signature (PITX3, DKK1, TLE1, LDHA) that robustly stratifies LUAD patients into high- and low-risk groups with significantly different survival outcomes. Notably, the signature also reflects distinct immune microenvironment landscapes, with high-risk patients exhibiting immunosuppressive features and elevated expression of immune checkpoint molecules.

The four genes identified have established roles in tumor biology. LDHA, a key glycolytic enzyme, promotes metabolic reprogramming and immune evasion in multiple cancers [15]. Its broad expression in our single-cell atlas, particularly in tumor epithelial and myeloid cells, aligns with its oncogenic functions. PITX3, a homeobox transcription factor, has been implicated in cell proliferation and differentiation; although its role in lung cancer remains underexplored, our data suggest it may serve as a novel prognostic factor [16]. DKK1, an antagonist of the Wnt/β-catenin pathway, contributes to tumor progression and immune modulation [17]. TLE1, a transcriptional corepressor, is associated with poor prognosis in various malignancies [18]. The convergence of these genes in a single signature underscores the multifaceted nature of LUAD pathogenesis, encompassing metabolism, development, and immune regulation.

Importantly, all four genes acted as risk factors (HR > 1), consistent with their reported oncogenic roles. The composite risk score may capture synergistic effects that enhance prognostic accuracy beyond individual genes. Our immune infiltration analyses further revealed that the high-risk group is characterized by an immunosuppressive microenvironment—enriched with M2 macrophages and mesenchymal stem cells, along with upregulated PDCD1, CTLA4, and LAG3—suggesting potential vulnerability to immune checkpoint blockade. Conversely, the low-risk group displayed higher abundances of effector immune cells ($CD8^+$ T cells, dendritic cells) indicative of an immune-active "hot" tumor milieu, which may correlate with better response to immunotherapy [19,20].

Despite these insights, several limitations should be acknowledged. The retrospective nature of TCGA data and the lack of an independent external validation cohort may affect generalizability. Although we validated expression patterns at single-cell resolution, functional experiments are required to elucidate the precise mechanisms by which these genes drive LUAD progression and immune evasion. Additionally, the predictive value of our signature for immunotherapeutic response warrants prospective evaluation in clinical cohorts receiving checkpoint inhibitors.

5. Conclusions

In summary, we developed and validated a four-gene prognostic signature (PITX3, DKK1, TLE1, LDHA) that effectively predicts overall survival and reflects the immune microenvironment in LUAD. This signature may serve as a promising biomarker for risk stratification and personalized immunotherapy. Further studies are warranted to translate these findings into clinical applications.

References

[1] GAO Q, LI P, JIANG X, et al. Worse disease-free, tumor-specific, and overall survival in surgically-resected lung adenocarcinoma patients with ALK rearrangement[J]. Oncotarget, 2017, 8(49): 86066-86081.

[2] VANSTEENKISTE J, WAUTERS E, REYMEN B, et al. Current status of immune checkpoint inhibition in early-stage NSCLC[J]. Annals of Oncology: Official Journal of the European Society for Medical Oncology, 2019, 30(8): 1244-1253.

[3] DENNEHY C, CONROY M R, FORDE P M. Immunotherapy for resectable lung cancer[J]. Cancer, 2025, 131(10): e35849.

[4] PAZ-ARES L, LUFT A, VICENTE D, et al. Pembrolizumab plus chemotherapy for squamous non-small-cell lung cancer[J]. The New England Journal of Medicine, 2018, 379(21): 2040-2051.

[5] HELLMANN M D, PAZ-ARES L, BERNABE CARO R, et al. Nivolumab plus ipilimumab in advanced non-small-cell lung cancer[J]. The New England Journal of Medicine, 2019, 381(21): 2020-2031.

[6] SPIGEL D R, FAIVRE-FINN C, GRAY J E, et al. Five-year survival outcomes from the PACIFIC trial: Durvalumab after chemoradiotherapy in stage III non-small-cell lung cancer[J]. Journal of Clinical Oncology: Official Journal of the American Society of Clinical Oncology, 2022, 40(12): 1301-1311.

[7] GALON J, BRUNI D. Approaches to treat immune hot, altered and cold tumours with combination immunotherapies[J]. Nature Reviews. Drug Discovery, 2019, 18(3): 197-218.

ISSN 2618-1584 Vol. 8, Issue 2: 49-58, DOI: 10.25236/FMSR.2026.080207

[8] CHENG C, CHEN W, JIN H, et al. A review of single-cell RNA-seq annotation, integration, and cell-cell communication[J]. Cells, 2023, 12(15): 1970.
[9] PETRONI G, FORMENTI S C, CHEN-KIANG S, et al. Immunomodulation by anticancer cell cycle inhibitors[J]. Nature Reviews Immunology, 2020, 20(11): 669-679.
[10] TRAYNOR S, JAKOBSEN M K, GREEN T M, et al. Single-cell sequencing unveils extensive intratumoral heterogeneity of cancer/testis antigen expression in melanoma and lung cancer[J]. Journal for Immunotherapy of Cancer, 2024, 12(6): e008759.
[11] BARRETT T, WILHITE S E, LEDOUX P, et al. NCBI GEO: Archive for functional genomics data sets--update[J]. Nucleic Acids Research, 2013, 41(Database issue): D991-995.
[12] LIBERZON A, BIRGER C, THORVALDSDÓTTIR H, et al. The molecular signatures database (MSigDB) hallmark gene set collection[J]. Cell Systems, 2015, 1(6): 417-425.
[13] COLAPRICO A, SILVA T C, OLSEN C, et al. TCGAbiolinks: An R/bioconductor package for integrative analysis of TCGA data[J]. Nucleic Acids Research, 2016, 44(8): e71.
[14] LUECKEN M D, THEIS F J. Current best practices in single-cell RNA-seq analysis: A tutorial[J]. Molecular Systems Biology, 2019, 15(6): e8746.
[15] SHARMA D, SINGH M, RANI R. Role of LDH in tumor glycolysis: Regulation of LDHA by small molecules for cancer therapeutics[J]. Seminars in Cancer Biology, 2022, 87: 184-195.
[16] TRAN T Q, KIOUSSI C. Pitx genes in development and disease[J]. Cellular and molecular life sciences: CMLS, 2021, 78(11): 4921-4938.
[17] SHI T, ZHANG Y, WANG Y, et al. DKK1 promotes tumor immune evasion and impedes anti-PD-1 treatment by inducing immunosuppressive macrophages in gastric cancer[J]. Cancer Immunology Research, 2022, 10(12): 1506-1524.
[18]YUAN D, YANG X, YUAN Z, et al. TLE1 function and therapeutic potential in cancer[J]. Oncotarget, 2017, 8(9): 15971-15976.
[19] WU B, ZHANG B, LI B, et al. Cold and hot tumors: From molecular mechanisms to targeted therapy[J]. Signal Transduction and Targeted Therapy, 2024, 9(1): 274.
[20] KHOSRAVI G R, MOSTAFAVI S, BASTAN S, et al. Immunologic tumor microenvironment modulators for turning cold tumors hot[J]. Cancer Communications, 2024, 44(5): 521-553.